# Monitoring Ultrafast Spin Crossover Intermediates in an Iron(II) Complex by Broad Band Stimulated X-ray Raman Spectroscopy

Yu Zhang,[†] Kochise Bennett,[§] and Shaul Mukamel*[ID]

Department of Chemistry, University of California, Irvine, California 92697, United States

S *Supporting Information*

ABSTRACT: The photoinduced spin crossover dynamics of transition metal complexes is of fundamental scientific importance and is used for sensor device applications and solar energy harvesting. Current X-ray and optical spectroscopy experiments for $[Fe^{II}(bpy)_3]$, an archetypal earth-abundant metal complex, show conflicting spin dynamics. We have simulated the broad band transient X-ray absorption and hybrid (broad + narrow band) X-ray stimulated Raman signals at the N and Fe K-edges of the key excited state intermediates involved in the spin crossover process of this complex. We find that these signals are much more sensitive to electron and spin populations than transition absorption and may be useful in the design of photovoltaic and artificial photosynthetic systems.
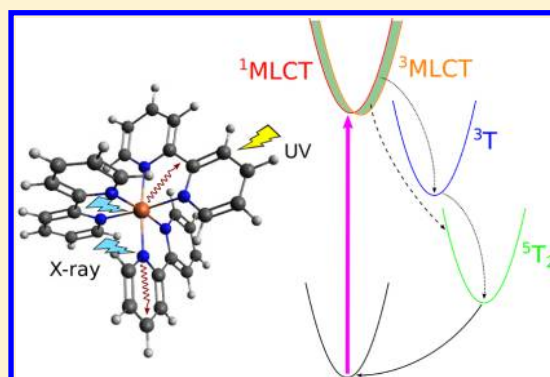
The photoinduced excited state dynamics of transition metal complexes are of fundamental interest with important applications in molecular electronics and solar cell technology. This dynamics usually involves an interplay of charge, spin, and molecular structure evolution.[1] Under light irradiation, transition metal complexes may undergo spin crossover (SCO)[2−4] transitions from low-spin (LS) to high-spin (HS) states. SCO materials are useful in light-controlled data storage.[5] More specifically, it is common to generate metal-to-ligand charge transfer singlet excited states (^{1}MLCT) in transition metal complexes using UV pulses, which rapidly evolve to metal-to-ligand charge transfer triplet states (^{3}MLCT) with very high quantum yields.[6] The ^{3}MLCT state plays a key role in the electron transfer dynamics since it hinders back-charge-transfer and facilitates further charge separation. However, the further decaying of the ^{3}MLCT state to the other metal-centered spin states in the SCO cascade competes with possible subsequent charge transfer processes. Hence SCO dynamics is an important factor to affect the photon energy harvesting yield of transition metal complexes, and it has been extensively investigated.

Time-resolved X-ray spectroscopy is a promising experimental technique for probing the photoinduced excited state dynamics in transition metal complexes due to its ability to probe of the local geometric and electronic structure of the metal center with high temporal resolution. Compared to conventional linear techniques such as X-ray absorption spectroscopy (XAS) and spontaneous X-ray emission spectroscopy (XES),[7] nonlinear X-ray spectroscopy techniques can probe the coupling between localized excitations around different sites in a molecule, thus providing sensitive detection windows for transient species.[8,9] Nonlinear X-ray experiments are becoming possible, thanks to the development of intense

ultrafast X-ray free electron laser sources.[10−16] The technique combines broad band and narrow band beams, and the resulting signals could resolve the ultrafast SCO dynamics and yield distinct signatures for different intermediates involved in the photoinduced SCO process and facilitate clean interpretation of the excited state dynamics in $[Fe^{II}(bpy)_3]$ and in other transition metal complexes.

Transition metal complexes are good candidates as photosensitizers in dye sensitized solar cells.[17−19] Considerable effort has been made in the search for efficient photosensitizers based on cheap earth-abundant metal complexes, such as Cu-[20−22] and Fe-complexes.[23−27] As an archetypal Fe-complex, $[Fe^{II}(bpy)_3]$ has been extensively studied by both experiment[28−40] and theory.[27,41−51] However, the SCO pathways have not been sorted out in detail. Figure 1 summarizes the photoinduced spin crossover dynamics derived from most recent experiments ((1)−(4) in the following) and spin−orbit coupling calculations. Different studies reported conflicting results: (1) Chergui and co-workers used time-resolved X-ray absorption spectroscopy at the Fe K-edge[31] and concluded that there is a direct intersystem crossing (ISC) step with a time constant ~120 fs from the ^{1,3}MLCT states to the $^5T_2$ state. (2) Gaffney and co-workers employed the time-resolved X-ray spontaneous emission spectroscopy (Fe Kβ) technique[36] and suggested that the ISC process consists of two steps with the time constants of 150 and 70 fs, respectively (see Figure 1), and there is an intermediate ^{3}T state between the ^{1,3}MLCT states and the $^5T_2$ state. (3) Recently, Chergui and co-workers utilized time-resolved UV spectroscopy[38] to study the same
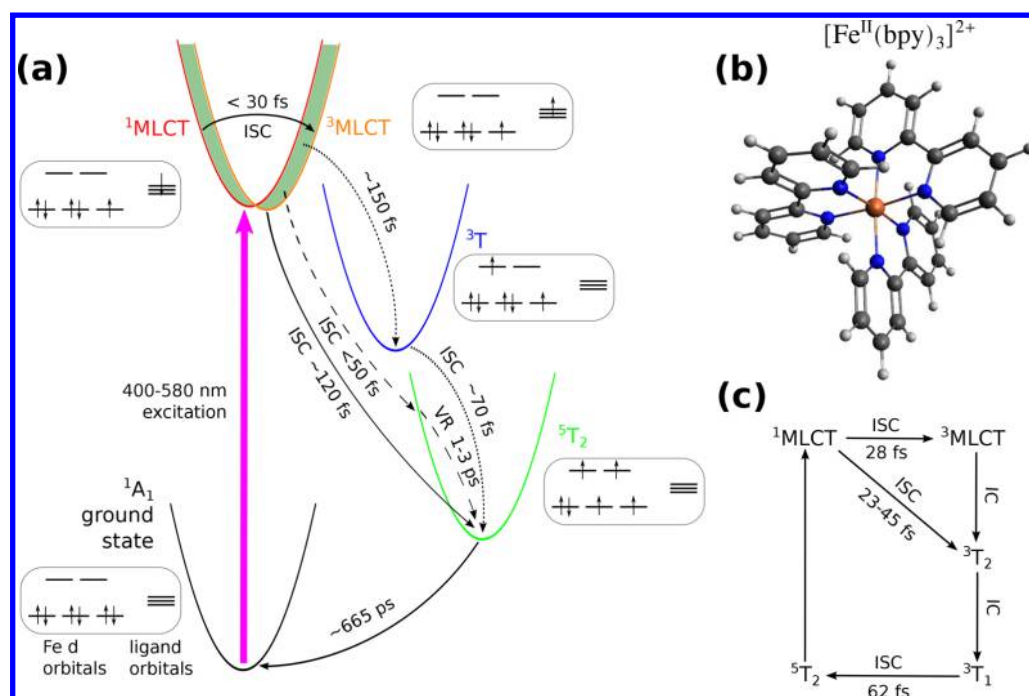
Figure 1. Photoinduced spin crossover dynamics in $[Fe^{II}(bpy)_3]^{2+}$. bpy = bipyridine. MLCT = metal-to-ligand charge transfer. ISC = intersystem crossing. IC = internal conversion. VR = vibrational relaxation. (a) Schematic summary of experimental spin crossover dynamics. The solid, dotted, and dashed arrows represent experimental results from refs 31, 36, and 38, respectively. Orbital schemes for the involved states are also shown. (b) Molecular structure of $[Fe^{II}(bpy)_3]^{2+}$. Color code: Fe, orange; N, blue; C, deep gray; H, light gray. (c) Schematic summary of the theoretical calculation results of the excited state dynamics in ref 47.

system. They found that some nontotally symmetric vibrational modes of the bpy ligand mediate the direct $^{1,3}MLCT \rightarrow$ $^3T_2$ transition, which means the $^{1,3}MLCT$ states decay to the vibrationally hot $^5T_2$ states in a sub-50 fs time scale and then relax to the vibrational ground state in 1.1−3.4 ps. (4) Aziz and co-workers used extreme ultraviolet (XUV) photoemission spectroscopy to study the SCO dynamics in this system again.[40] With the help of calculations, they demonstrated that the $^{1,3}MLCT$ states decay to the $^5T_2$ state with a combination of the sequential (via the ^3T intermediate states) and the direct pathways (without the intermediate states). (5) On the basis of the CASPT2 excited state energy and spin−orbit coupling calculations,[47] Sousa et al. found more intermediate energy states ($^3T_1$ and $^3T_2$) and more complex spin crossover dynamics, which combines ISC with internal conversion (IC) processes (Figure 1c). They concluded that the direct $^{1,3}MLCT \rightarrow {}^3T_2$ transition is unlikely due to the very weak spin−orbit coupling between these two states, as the transition involves the simultaneous movement of two electrons and spin flips. Their transition rate calculations relied on the assumption that vibrational cooling is faster than intersystem crossing, and they argued that including higher vibrational levels would not change the overall picture of the SCO dynamics.

The major challenge in unambiguously resolving the SCO pathways is detecting the possible intermediate states with high temporal resolution. Previous experiments[31,36,38] showed that a time resolution below 60 fs is necessary to reveal the excited state cascade. The intersystem crossing $^1MLCT \rightarrow {}^3MLCT$ is extremely fast (<30 fs), and the common $K\beta$ mainline X-ray emission technique is not sensitive to ligands,[36] since it mainly studies the metal 3d to 1s transitions. Transient optical absorption spectroscopy cannot resolve the intermediate state dynamics since the involved transitions are spin-forbidden and

overlap with other allowed charge transfer transitions.[35] An ideal spectroscopic technique for resolving the dynamics should give distinct spectral patterns for each species, so that the results do not heavily rely on numerical fitting to some kinetic model. In short, powerful spectroscopic tools with both high temporal resolution and chemical sensitivity are called for.

The complex dynamics involving charge, spin, and structural changes in photoexcited $[Fe^{II}(bpy)_3]^{2+}$ is too difficult for an *ab initio* quantum dynamics simulation at the current level of quantum chemistry theory and computational power. For simplicity we fix the complex at its ground state geometry and study the X-ray spectroscopy signals of different spin states. Since the ISC processes in this Fe-complex happen in a ∼100 fs or less, their detection requires faster spectroscopic techniques. We compare the following X-ray techniques:

- X-ray transient absorption (XTA) with broad band pulses (eq 1). This simplest time-resolved spectroscopy technique is used as a reference. We use a broad band pulse to achieve the femtosecond time resolution necessary to observe the ^1MLCT to ^3MLCT spin flip dynamics. The broad spectral band of such pulses allows us to measure a wide region of the spectrum in a single shot.

- Hybrid band stimulated X-ray Raman spectroscopy (HSXRS)[52] (eq 2), also known as attosecond stimulated Raman spectroscopy (ASRS).[53,54] This is an X-ray analogue of femtosecond stimulated Raman spectroscopy (FSRS)[55] in the optical regime. In this technique, a higher-energy (long, narrow band) pump pulse and a lower-energy (short, broad band) probe pulse arrive at the sample at the same time, creating a superposition of valence excited states through an X-ray Raman process. This hybrid narrow/broad band combination improves

the combined spectral and temporal resolution. The theoretical description of HSXRS has been presented in refs 52 and 54. Another X-ray Raman pump–probe technique, stimulated X-ray Raman spectroscopy (SXRS),[56,57] only uses a broad band probe and usually requires over 100 fs of pulse delay to achieve adequate frequency resolution.[53] HSXRS does not have this time restriction and should be suitable for probing ultrafast dynamics.

We use the following expressions to calculate the frequency-dispersed XTA and HSXRS signals[52] in the study (see the Supporting Information for theoretical details):

$$S_{XTA}^{(fd)}(\omega_s,T) = \mathcal{S}[\alpha_{gg}^{(00)}(\omega_s,T)] \tag{1}$$

$$S_{HSXRS}^{(fd)}(\omega_s,\Delta_s,T)$$
$$= -\mathcal{R}\left[\sum_c \frac{\alpha_{cg}^{(01)}(T)\,\alpha_{cg}^{(10)}(T) - \alpha_{cg}^{(01)}(T)\,\alpha_{cg}^{(01)*}(T)}{\Delta_s - \omega_{cg}(T) + i\Gamma_c}\right] \tag{2}$$

Here, T is the delay time between the UV pump pulse and the X-ray probe pulses, g is the ground state, c is the valence excited state index, Γ_c is the lifetime broadening of state c, ω_s is the detected frequency, ω_1 is the narrow-band frequency, $\Delta_s = \omega_s - \omega_1$ is the Raman shift, the superscripts 0 and 1 stand for the broad or the narrow-band pulse, respectively, and $\mathcal{R}$ and $\mathcal{S}$ denote the real and imaginary part, respectively. $\alpha(\omega,T)$ is the frequency-dependent polarizability. $\alpha(T)$ is obtained by integrate the frequency out of $\alpha(\omega,T)$. The derivation of the equations above and the details of the quantum chemistry calculations to obtain the quantities in the equations can be found in Supporting Information. The calculated signals represent snapshots at fixed geometries at time T of the four species of interest and so the time dependence of the signals are not shown.

The normalized XTA spectra at the N and Fe K-edges for the ^{1,3}MLCT and ^{3,5}T states of $[Fe^{II}(bpy)_3]^{2+}$ are calculated and shown in Figure 2. We use a broad band probe (Gaussian pulse shape with $\sigma = 5$ eV) since an ultrafast pulse will be necessary to capture the femtosecond dynamics.

Due to the large lifetime line broadening ($\gamma_{Fe} \approx 1.5$ eV), the Fe K-edge XTA does not spectrally resolve the two MLCT and metal-centered states. MLCT states have a strong feature around 6982.5 eV, which corresponds to a core excitation to molecular orbitals on the four pyridine rings with C and H s orbital character. The two metal-centered states ^{3}T and ^{5}T both have strong features around 6979.3, 6984.7, and 6987.4 eV. The 6979.3 features are similar to the 6982.5 eV features of the MLCT states, while the 6984.7 and 6987.4 eV features carry some Rydberg state character. The spectra of ^{3}T and ^{5}T only show some fine structure differences, which requires high resolution. The calculated oscillator intensities (au) of the strongest peaks of ^{1}MLCT, ^{3}MLCT, ^{3}T, and ^{5}T are 0.0030, 0.00019, 0.00034, and 0.00038, respectively. Thus, ^{1}MLCT has much stronger X-ray absorption than the other three species, hence in a real XTA experiment the signals of ^{3}MLCT, ^{3}T, and ^{5}T could easily be overwhelmed by the signal of ^{1}MLCT.

Although the overall shapes of the nitrogen K-edge XTA spectra are very similar for the two MLCT states (left column in Figure 2), the much smaller lifetime broadening ($\gamma_N = 0.09$ eV) allows a better spectral resolution. The ^{1}MLCT state shows one strong peak at 388.9 eV and a weaker peak around
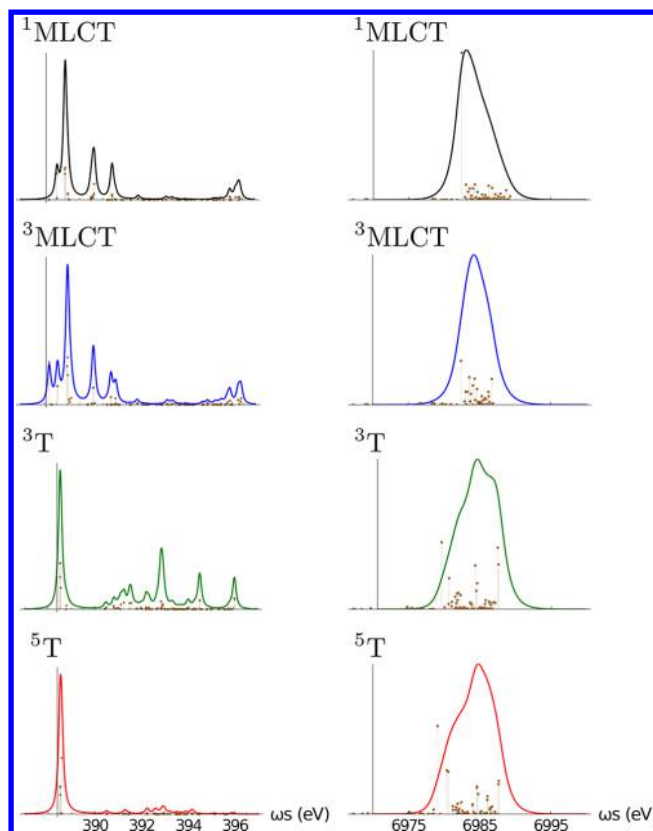

Figure 2. Normalized X-ray transient absorption at the nitrogen (left column) and iron (right column) K-edges for the four species: MLCT singlet (black), MLCT triplet (blue), triplet (orange), and quintet (red). Oscillator strengths are included as stick spectra. Simulations utilize Gaussian pulses with 393 and 6985 eV carrier frequencies for N 1s and Fe 1s edges, respectively. A 5 eV bandwidth (standard deviation) is used for all pulses.

388.5 eV. These correspond to core excitations from the N 1s orbital to the π^* orbitals on the bipyridine ligand which contains the excited N atom. However, for the ^{3}MLCT state, an entirely new spectral line appears at roughly 388.2 eV. This corresponds to an N 1s core excitation to the π^* orbitals on two bipyridine ligands, which is more delocalized than the 388.5 and 388.9 eV excitations. This new peak, not seen in the MLCT singlet state, can be used to clearly track the spin dynamics of the charge-transfer state. The absorption from the ^{3}T and ^{5}T states is very different. Most prominently, the nitrogen spectrum of ^{3}T possesses three strong peaks, at ≈ 392.9, ≈ 394.5, and ≈ 396.0 eV, which are missing for ^{5}T. These peaks also represent N 1s core excitation to a single bipyridine ligand. The calculated oscillator intensities (au) of the strongest peaks of ^{1}MLCT, ^{3}MLCT, ^{3}T, and ^{5}T are 0.040, 0.042, 0.046, and 0.083, respectively. All species therefore have comparable nitrogen K-edge X-ray absorptions and the selective detection of this signal for each species is possible.

Resonant X-ray absorption spectroscopy probes unoccupied orbitals. In our system, the SCO dynamics happens mostly on the ligands, and the transition dipoles between the metal core orbital and ligand unoccupied orbitals are very small, which implies that the XTA signals at the Fe K-edge are not sensitive to the SCO dynamics. In addition, as mentioned above, the short lifetime of the iron 1s core hole also leads to low resolution of the absorption spectral features. We have already shown Fe K-edge XTA signals (Figure 2) are not selective for
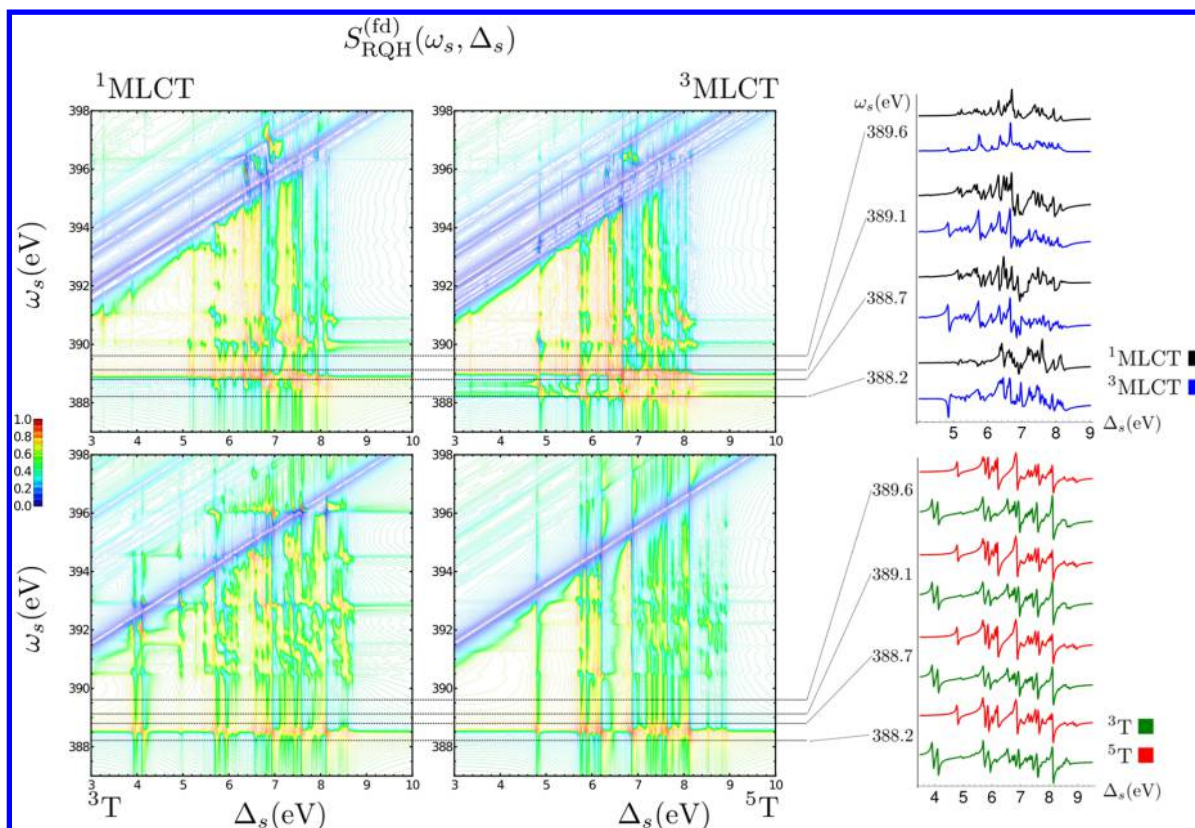
Figure 3. Normalized nitrogen K-edge resonant quadratic HSXRS signal for four species of $[Fe^{II}(bpy)_3]^{2+}$ using a Gaussian pulse with central frequency at the Nitrogen 1s core (ω_{s0} = 393 eV) and width σ = 5 eV. Vertical axes are the detected (signal) frequency and horizontal axes are the Raman shifts $\Delta_s = \omega_s - \omega_1$ between detected and narrow-band frequencies. Calculations are done using eq 2.

those spin states. Different from X-ray absorption, stimulated X-ray Raman signals represent how core holes couple via valence unoccupied orbitals. Although these quadratic signals are usually much weaker than the linear XTA signals, they are more sensitive to small changes in the local electronic structure of the exited atoms for their higher-order response character. Furthermore, similar to the optical Raman spectroscopy, X-ray Raman has a better spectral resolution than X-ray absorption because of the longer lifetime of the valence excited final state. We have already shown Fe K-edge XTA signals are not selective for those spin states. Compared to XTA at the N K-edge, HSXRS at Fe K-edge has advantages in higher temporal resolution and less photodamage because of the hard X-ray used. In Figures 3 and 4, we show the HSXRS signal (eq 2) for the four selected species of $[Fe^{II}(bpy)_3]^{2+}$ at the nitrogen and iron K-edges, respectively. This signal employs a hybrid broad band-narrow band probe pulse and is quadratic in the probe intensity. In all cases, the broad band pulse has a bandwidth of 5 eV while the narrow band pulse is taken to be monochromatic. This signal shows valence electronic rather than core resonances. The former have much narrower lifetime broadening and hence better spectral resolution. In addition, it has high temporal and spectral resolutions. In Figures 3 and 4, we plot the excitation energy vs the Raman shift (y:x). Features on a horizontal line have the same (core) excitation energy, vertical lines mean fixed final (valence excited) state energies, and diagonal lines imply constant emission energies.

Although XTA could distinguish the four species to some extent, we can see greater differences in the X-ray Raman signals shown in Figure 3. For example, the three horizontal lines at $\omega_s \approx$ 388.9, 388.5, and 388.2 eV in the ^{3}MLCT spectra are characteristic to that species. The ^{1}MLCT spectrum possesses similar features on the $\omega_s \approx$ 388.9 eV line while the other two lines show weak features. The ^{3}T and ^{5}T spectra also possess features on the $\omega_s \approx$ 388.5 eV line but the triple-line structure is unique to the ^{3}MLCT state. The ^{3}T state has features around the 4 eV vertical line, which are absent in ^{5}T. The valence excited states around 4 eV represent excitations from the Fe−N d−π σ bond orbital to the π^* orbitals on the bipyridine ligands. The ^{3}T and ^{5}T species can be distinguished by the presence of several peaks beside the diagonal blue band in the spectra of the former. The signal differences can be clearly seen from horizontal slices of the 2D plots in Figure 3. Those slices are given in the Supporting Information. These are successive spectra of the Raman shift Δ_s, each at a fixed detected frequency ω_s. Unlike ^{1}MLCT, ^{3}MLCT has significant features below Δ_s = 5 eV, and the ^{3}T state has Raman activity around Δ_s = 4.8 eV but the ^{5}T state has features around Δ_s = 4 eV. Other types of slices that emphasize the differences of the signal patterns of various species are possible. These flexible slice choices can be used to obtain an optimal global fitting for the transient signals, which leads to an improved identification of SCO intermediates and pathways.

Figure 4 shows the HSXRS signal at the Fe K-edge. Unlike the N 1s spectra, we find no obvious horizontal and diagonal patterns. This may indicate a more intricate core−valence excited state coupling at the Fe K-edge. We have seen in Figure 2 that the broad iron core-hole excitations rendered the XTA spectra far less distinct and informative than at the nitrogen K-edge. It is here that the hybrid Raman signal shows its power,
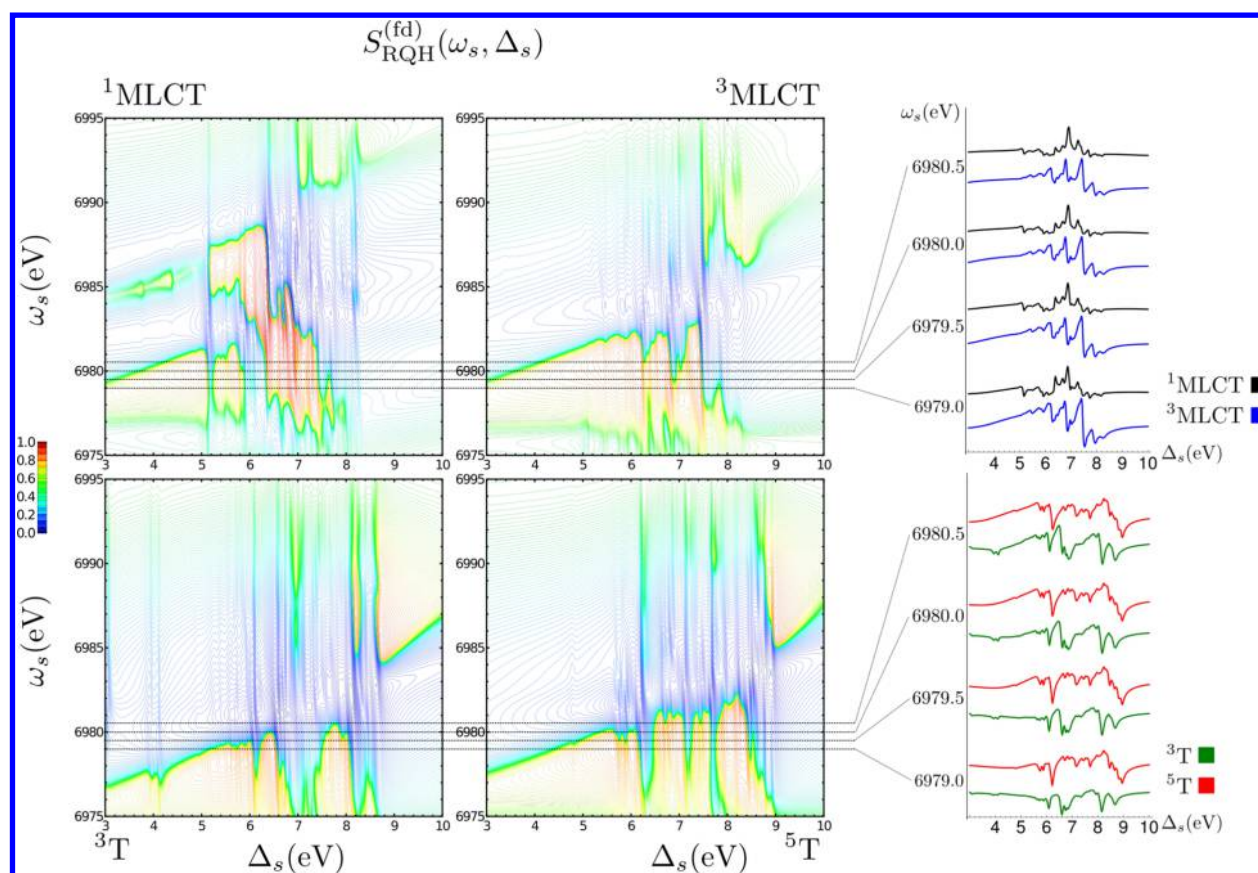
Figure 4. Normalized Fe K-edge resonant quadratic HSXRS signal for the four species of $[Fe^{II}(bpy)_3]^{2+}$ using a Gaussian pulse with central frequency at the iron 1s core ($\omega_{s0} = 6985$ eV) and width $\sigma = 5$ eV. Vertical axes are the detected (signal) frequency and horizontal axes are the Raman shifts $\omega_s - \omega_1$ between detected and narrow-band frequencies.

as the resulting spectra can easily distinguish the four species. Noticeably, the ^{1}MLCT state possesses a prominent peak in the center of the spectra ($\omega_s \approx 6982.5$ eV, $\Delta_s \approx 6.4$ eV) where the signal from the other species virtually vanishes. Although there are strong XTA features around 6982.5 eV for the ^{1}MLCT state, its hybrid Raman spectrum lacks features along the 6982.5 eV horizontal line. The regions $6977 \lesssim \omega_s \lesssim 6983$ and $6 \lesssim \Delta_s \lesssim 8.5$ show very comoplicated structures of features that may provide a fingerprint region capable of distinguishing the remaining three spectra. For example, there are no significant features around the 7.0 eV vertical line in the ^{3}T spectrum, while all the other species have some features at certain core excitation energies. A sequence of horizontal slices are shown in the right panel of Figure 4. One can see the ^{1}MLCT state mostly differs from ^{3}MLCT at $\Delta_s \approx 5$ and 6 eV, and the ^{3}T state differs from the ^{5}T state the most at $\Delta_s \approx 6.8$ and 8.2 eV.

We have compared the X-ray transient absorption and hybrid band stimulated X-ray Raman signals of the Fe(II) bipyridine complex species involved in its photoinduced ultrafast spin-crossover dynamics. We find that the Fe K-edge broad band X-ray absorption signals are not very different for these species because of the short lifetime of the Fe 1s core hole. In contrast the X-ray absorption signals at the K-edges of the N atoms on the bipyridine ligands can be used to distinguish the excited state species. The smaller lifetime broadening of the N 1s core hole results in well-resolved spectra even for pulses of a few-electronvolt bandwidth. More importantly, the simulated hybrid band stimulated X-ray

Raman signals, which are quadratic in the intensity of the incident light field, are more sensitive to the subtle changes of electronic structure and spin of the system. Both N 1s and Fe 1s hybrid band X-ray Raman signals show a notable variance for the four excited state species studied. The better resolution of the Raman spectra are due to the smaller dephasing rates of Raman resonances, allowing the use of even very short-lived core states as intermediares for the valence excitation. Conventional linear spectroscopy does not produce very distinct signal patterns for those species.[31,36,38] The current study shows that the hybrid band stimulated X-ray Raman technique may be used to study the spin-crossover dynamics at a high level of accuracy, and identify ultrafast spin-crossover pathways in transition metal complexes.

In this study, we have focused on K-edge spectroscopies with hard X-rays. In contrast, the L-edge spectroscopies in the soft X-ray energy regime have the advantage that the involved transitions are dipole allowed, the more chemically relevant metal d orbitals are directly probed, and the corresponding spectral resolutions are better (for longer core-hole lifetime) than those of K-edge spectroscopies. However, L-edge spectroscopy techniques in molecules are very challenging because of photodamage, low sample concentration in solution, large absorption and emission background from light atoms, and ultrahigh vacuum experimental condition requirements. Through element-specific partial fluorescence yield (PFY) detection, L-edge X-ray absorption spectroscopy measurements were recently made possible for metalloproteins at mild experimental condition with X-ray free electron

lasers.[58,59] L-edge spectroscopies are more sensitive than K-edge spectroscopies since the open-shell d orbitals are directly probed. Thus, when they become possible, L-edge absorption, emission, resonant inelastic X-ray scattering, and stimulated X-ray Raman spectroscopies may provide complementary information on the spin state evolution in transition metal complexes and deepen our understanding of the corresponding SCO dynamics.

Previous X-ray emission spectroscopy experiments (Fe Kβ mainline)[36] could not directly access the MLCT states, since the involved excitations are metal-centered and not sensitive to the ligands. However, valence-to-core X-ray emission (VtC-XES) spectroscopy[60,61] can probe the geometries and electronic structures of ligands. Conventional VtC-XES measures the spontaneous X-ray emission transition from the ligand orbitals to the metal core hole of the system after a core ionization. An experimental difficulty of this technique is that the signals are weak. Special care must be taken in order to extract the desired weak features out of the long decaying tails of the much stronger Kβ mainline features.[60] To remedy this difficulty, one can use another X-ray pulse designed to stimulate the emission in a certain valence-to-core energy region, thus enhancing the corresponding weak spontaneous emission features. Stimulated VtC-XES could be broadly applied and become a general technique to increase the chemical sensitivity of conventional spontaneous VtC-XES. However, the large broadening of the VtC-XES features caused by the short core-hole lifetime severely limits the spectral resolution. A large amplification of certain features would introduce a narrowing and it might be possible to overcome the limit of core-hole lifetime broadening.

Stimulated X-ray emission or Raman experiments have been made possible with X-ray free electron laser (XFEL) for atoms and diatomic molecules.[62−67] The signals require stable attosecond pulses with controlled time separation and competing processes[67] may complicate the interpretation for larger molecules. With the fast development of XFEL, these difficulties could be overcome and stimulated X-ray hybrid band Raman experiments on transition metal complexes are expected in the near future.

ASSOCIATED CONTENT

Ⓢ Supporting Information

The Supporting Information is available free of charge on the ACS Publications website at DOI: 10.1021/acs.jpca.8b01762.

Loop diagrams of the frequency-dispersed XTA and HSXRS signals, additional notes about the derivation of the signal expressions, computational methods, calculated energies of studied excited states, and spin density difference plots (PDF)

AUTHOR INFORMATION

Corresponding Author

*S. Mukamel. E-mail: smukamel@uci.edu.

ORCID Ⓘ

Kochise Bennett: 0000-0002-9224-6088

Shaul Mukamel: 0000-0002-6015-3135

Present Addresses

†SLAC National Accelerator Laboratory, 2575 Sand Hill Rd, Menlo Park, CA 94025, USA.

§UC Berkeley, 260 Stanley Hall, Berkeley, CA 94709, USA

REFERENCES

(1) Chergui, M. On the Interplay between Charge, Spin and Structural Dynamics in Transition Metal Complexes. *Dalton Trans.* **2012**, *41*, 13022−13029.

(2) Gütlich, P., Goodwin, H. A., Eds. *Spin Crossover in Transition Metal Compounds I-III*; Topics in Current Chemistry; Springer: Berlin, Heidelberg, 2004; Vols. *233−235*.

(3) Bousseksou, A.; Molnár, G.; Salmon, L.; Nicolazzi, W. Molecular Spin Crossover Phenomenon: Recent Achievements and Prospects. *Chem. Soc. Rev.* **2011**, *40*, 3313−3335.

(4) Halcrow, M. A., Ed. *Spin-Crossover Materials: Properties and Applications*; Wiley-Blackwell, 2013.

(5) Gütlich, P. In *Spin Crossover in Transition Metal Compounds I*; Gütlich, P., Goodwin, H. A., Eds.; Topic in Current Chemistry; Springer: Berlin, Heidelberg, 2004; Vol. *233*, Chapter 1, pp 1−47.

(6) Saes, M.; Bressler, C.; Abela, R.; Grolimund, D.; Johnson, S. L.; Heimann, P. A.; Chergui, M. Observing Photochemical Transients by Ultrafast X-Ray Absorption Spectroscopy. *Phys. Rev. Lett.* **2003**, *90*, 047403.

(7) van Bokhoven, J. A., Lamberti, C., Eds. *X-Ray Absorption and X-Ray Emission Spectroscopy: Theory and Applications*; John Wiley & Sons: Chichester, U.K., 2016.

(8) Zhang, Y.; Hua, W.; Bennett, K.; Mukamel, S. In *Density-Functional Methods for Excited States*; Ferré, N., Filatov, M., Huix-Rotllant, M., Eds.; Topics in Current Chemistry; Springer International Publishing: Switzerland, 2016; Vol. *368*; Chapter 7, pp 273−345.

(9) Bennett, K.; Zhang, Y.; Kowalewski, M.; Hua, W.; Mukamel, S. Multidimensional Resonant Nonlinear Spectroscopy with Coherent Broadband X-ray Pulses. *Phys. Scr.* **2016**, *T169*, 014002.

(10) Lutman, A. A.; Coffee, R.; Ding, Y.; Huang, Z.; Krzywinski, J.; Maxwell, T.; Messerschmidt, M.; Nuhn, H.-D. Experimental Demonstration of Femtosecond Two-Color X-Ray Free-Electron Lasers. *Phys. Rev. Lett.* **2013**, *110*, 134801.

(11) Lutman, A. A.; Decker, F.-J.; Arthur, J.; Chollet, M.; Feng, Y.; Hastings, J.; Huang, Z.; Lemke, H.; Nuhn, H.-D.; Marinelli, A.; et al. Demonstration of Single-Crystal Self-Seeded Two-Color X-Ray Free-Electron Lasers. *Phys. Rev. Lett.* **2014**, *113*, 254801.

(12) Marcus, G.; Penn, G.; Zholents, A. A. Free-Electron Laser Design for Four-Wave Mixing Experiments with Soft-X-Ray Pulses. *Phys. Rev. Lett.* **2014**, *113*, 024801.

(13) Petralia, A.; Anania, M. P.; Artioli, M.; Bacci, A.; Bellaveglia, M.; Carpanese, M.; Chiadroni, E.; Cianchi, A.; Ciocci, F.; Dattoli, G.; et al. Two-Color Radiation Generated in a Seeded Free-Electron Laser with Two Electron Beams. *Phys. Rev. Lett.* **2015**, *115*, 014801.

(14) Ratner, D.; Abela, R.; Amann, J.; Behrens, C.; Bohler, D.; Bouchard, G.; Bostedt, C.; Boyes, M.; Chow, K.; Cocco, D.; et al. Experimental Demonstration of a Soft X-Ray Self-Seeded Free-Electron Laser. *Phys. Rev. Lett.* **2015**, *114*, 054801.

(15) Wu, Y. K.; Yan, J.; Hao, H.; Li, J. Y.; Mikhailov, S. F.; Popov, V. G.; Vinokurov, N. A.; Huang, S.; Wu, J. Widely Tunable Two-Color

Free-Electron Laser on a Storage Ring. *Phys. Rev. Lett.* **2015**, *115*, 184801.

(16) Roussel, E.; Ferrari, E.; Allaria, E.; Penco, G.; Di Mitri, S.; Veronese, M.; Danailov, M.; Gauthier, D.; Giannessi, L. Multicolor High-Gain Free-Electron Laser Driven by Seeded Microbunching Instability. *Phys. Rev. Lett.* **2015**, *115*, 214801.

(17) Hagfeldt, A.; Boschloo, G.; Sun, L.; Kloo, L.; Pettersson, H. Dye-Sensitized Solar Cells. *Chem. Rev.* **2010**, *110*, 6595–6663.

(18) Bignozzi, C.; Argazzi, R.; Boaretto, R.; Busatto, E.; Carli, S.; Ronconi, F.; Caramori, S. The Role of Transition Metal Complexes in Dye Sensitized Solar Devices. *Coord. Chem. Rev.* **2013**, *257*, 1472–1492.

(19) Baranoff, E. In *Organometallics and Related Molecules for Energy Conversion*; Wong, W.-Y., Ed.; Springer: Berlin, Heidelberg, 2015; Chapter 3, pp 61–90.

(20) McCusker, C. E.; Castellano, F. N. Design of a Long-Lifetime, Earth-Abundant, Aqueous Compatible Cu(I) Photosensitizer Using Cooperative Steric Effects. *Inorg. Chem.* **2013**, *52*, 8114–8120.

(21) Lazorski, M. S.; Castellano, F. N. Advances in the Light Conversion Properties of Cu(I)-based Photosensitizers. *Polyhedron* **2014**, *82*, 57–70.

(22) Housecroft, C. E.; Constable, E. C. The Emergence of Copper(I)-based Dye Sensitized Solar Cells. *Chem. Soc. Rev.* **2015**, *44*, 8386–8398.

(23) Ferrere, S.; Gregg, B. A. Photosensitization of TiO2 by [Fe(II)(2,2′-bipyridine-4,4′-dicarboxylic acid)2(CN)2]: Band Selective Electron Injection from Ultra-Short-Lived Excited States. *J. Am. Chem. Soc.* **1998**, *120*, 843–844.

(24) Monat, J. E.; McCusker, J. K. Femtosecond Excited-State Dynamics of an Iron(II) Polypyridyl Solar Cell Sensitizer Model. *J. Am. Chem. Soc.* **2000**, *122*, 4092–4097.

(25) Mukherjee, S.; Bowman, D. N.; Jakubikova, E. Cyclometalated Fe(II) Complexes as Sensitizers in Dye-Sensitized Solar Cells. *Inorg. Chem.* **2015**, *54*, 560–569.

(26) Harlang, T. C. B.; Liu, Y.; Gordivska, O.; Fredin, L. A.; Ponseca, C. S.; Huang, P.; Chábera, P.; Kjaer, K. S.; Mateos, H.; Uhlig, J.; et al. Iron Sensitizer Converts Light to Electrons with 92% Yield. *Nat. Chem.* **2015**, *7*, 883–889.

(27) Jakubikova, E.; Bowman, D. N. Fe(II)-Polypyridines as Chromophores in Dye-Sensitized Solar Cells: A Computational Perspective. *Acc. Chem. Res.* **2015**, *48*, 1441–1449.

(28) Creutz, C.; Chou, M.; Netzel, T. L.; Okumura, M.; Sutin, N. Lifetimes, Spectra, and Quenching of the Excited states of Polypyridine Complexes of Iron(II), Ruthenium(II), and Osmium-(II). *J. Am. Chem. Soc.* **1980**, *102*, 1309–1319.

(29) McCusker, J. K.; Walda, K. N.; Dunn, R. C.; Simon, J. D.; Magde, D.; Hendrickson, D. N. Subpicosecond ^{1}MLCT -^{5}T$_2$ Intersystem Crossing of Low-spin Polypyridyl Ferrous Complexes. *J. Am. Chem. Soc.* **1993**, *115*, 298–307.

(30) Gawelda, W.; Cannizzo, A.; Pham, V.-T.; van Mourik, F.; Bressler, C.; Chergui, M. Ultrafast Nonadiabatic Dynamics of [Fe(II)(bpy)$_3$]$^{2+}$ in Solution. *J. Am. Chem. Soc.* **2007**, *129*, 8199–8206.

(31) Bressler, C.; Milne, C.; Pham, V.-T.; ElNahhas, A.; van der Veen, R. M.; Gawelda, W.; Johnson, S.; Beaud, P.; Grolimund, D.; Kaiser, M.; et al. Femtosecond XANES Study of the Light-Induced Spin Crossover Dynamics in An Iron(II) Complex. *Science* **2009**, *323*, 489–492.

(32) Consani, C.; Prémont-Schwarz, M.; ElNahhas, A.; Bressler, C.; van Mourik, F.; Cannizzo, A.; Chergui, M. Vibrational Coherences and Relaxation in the High-Spin State of Aqueous [Fe(II)(bpy)$_3$]$^{2+}$. *Angew. Chem., Int. Ed.* **2009**, *48*, 7184–7187.

(33) Cannizzo, A.; Milne, C.; Consani, C.; Gawelda, W.; Bressler, C.; van Mourik, F.; Chergui, M. Light-induced Spin Crossover in Fe(II)-based Complexes: The Full Photocycle Unraveled by Ultrafast Optical and X-ray Spectroscopies. *Coord. Chem. Rev.* **2010**, *254*, 2677–2686.

(34) Cho, H.; Strader, M. L.; Hong, K.; Jamula, L.; Gullikson, E. M.; Kim, T. K.; de Groot, F. M. F.; McCusker, J. K.; Schoenlein, R. W.;

Huse, N. Ligand-field Symmetry Effects in Fe(II) Polypyridyl Compounds Probed by Transient X-ray Absorption Spectroscopy. *Faraday Discuss.* **2012**, *157*, 463–474.

(35) Lemke, H. T.; Bressler, C.; Chen, L. X.; Fritz, D. M.; Gaffney, K. J.; Galler, A.; Gawelda, W.; Haldrup, K.; Hartsock, R. W.; Ihee, H.; et al. Femtosecond X-ray Absorption Spectroscopy at a Hard X-ray Free Electron Laser: Application to Spin Crossover Dynamics. *J. Phys. Chem. A* **2013**, *117*, 735–740.

(36) Zhang, W.; Alonso-Mori, R.; Bergmann, U.; Bressler, C.; Chollet, M.; Galler, A.; Gawelda, W.; Hadt, R. G.; Hartsock, R. W.; Kroll, T.; et al. Tracking Excited-state Charge and Spin Dynamics in Iron Coordination Complexes. *Nature* **2014**, *509*, 345–348.

(37) Zhang, W.; Gaffney, K. J. Mechanistic Studies of Photoinduced Spin Crossover and Electron Transfer in Inorganic Complexes. *Acc. Chem. Res.* **2015**, *48*, 1140–1148.

(38) Auböck, G.; Chergui, M. Sub-50-fs Photoinduced Spin Crossover in [Fe(bpy)$_3$]$^{2+}$. *Nat. Chem.* **2015**, *7*, 629–633.

(39) Miaja-Avila, L.; O'Neil, G. C.; Joe, Y. I.; Alpert, B. K.; Damrauer, N. H.; Doriese, W. B.; Fatur, S. M.; Fowler, J. W.; Hilton, G. C.; Jimenez, R.; et al. Ultrafast Time-Resolved Hard X-Ray Emission Spectroscopy on a Tabletop. *Phys. Rev. X* **2016**, *6*, 031047.

(40) Moguilevski, A.; Wilke, M.; Grell, G.; Bokarev, S. I.; Aziz, S. G.; Engel, N.; Raheem, A. A.; Kühn, O.; Kiyan, I. Y.; Aziz, E. F. Ultrafast Spin Crossover in [Fe^{II} (bpy)$_3$]$^{2+}$: Revealing Two Competing Mechanisms by Extreme Ultraviolet Photoemission Spectroscopy. *ChemPhysChem* **2017**, *18*, 465–469.

(41) Lawson Daku, L. M.; Vargas, A.; Hauser, A.; Fouqueau, A.; Casida, M. E. Assessment of Density Functionals for the High-Spin/Low-Spin Energy Difference in the Low-Spin Iron(II) Tris(2,2′-bipyridine) Complex. *ChemPhysChem* **2005**, *6*, 1393–1410.

(42) de Graaf, C.; Sousa, C. Study of the Light-Induced Spin Crossover Process of the [Fe(II)(bpy)$_3$]$^{2+}$ Complex. *Chem. - Eur. J.* **2010**, *16*, 4550–4556.

(43) Lawson Daku, L. M.; Hauser, A. ab Initio Molecular Dynamics Study of an Aqueous Solution of [Fe(bpy)$_3$]Cl$_2$ in the Low-Spin and in the High-Spin States. *J. Phys. Chem. Lett.* **2010**, *1*, 1830–1835.

(44) de Graaf, C.; Graaf; Sousa, C. On the Role of the Metal-to-ligand Charge Transfer States in the Light-induced Spin Crossover in Fe(II)(bpy)$_3$. *Int. J. Quantum Chem.* **2011**, *111*, 3385–3393.

(45) Iuchi, S. A Model Electronic Hamiltonian to Study Low-lying Electronic States of [Fe(bpy)$_3$]$^{2+}$ in Aqueous Solution. *J. Chem. Phys.* **2012**, *136*, 064519.

(46) Bowman, D. N.; Jakubikova, E. Low-Spin versus High-Spin Ground State in Pseudo-Octahedral Iron Complexes. *Inorg. Chem.* **2012**, *51*, 6011–6019.

(47) Sousa, C.; de Graaf, C.; Rudavskyi, A.; Broer, R.; Tatchen, J.; Etinski, M.; Marian, C. M. Ultrafast Deactivation Mechanism of the Excited Singlet in the Light-Induced Spin Crossover of [Fe(2,2′-bipyridine)$_3$]$^{2+}$. *Chem. - Eur. J.* **2013**, *19*, 17541–17551.

(48) Pápai, M.; Vankó, G.; de Graaf, C.; Rozgonyi, T. Theoretical Investigation of the Electronic Structure of Fe(II) Complexes at Spin-State Transitions. *J. Chem. Theory Comput.* **2013**, *9*, 509–519.

(49) Johnson, P. S.; Cook, P. L.; Zegkinoglou, I.; García-Lastra, J. M.; Rubio, A.; Ruther, R. E.; Hamers, R. J.; Himpsel, F. J. Electronic Structure of Fe- vs. Ru-based Dye Molecules. *J. Chem. Phys.* **2013**, *138*, 044709.

(50) Iuchi, S.; Koga, N. An Improved Model Electronic Hamiltonian for Potential Energy Surfaces and Spin-orbit Couplings of Low-lying d-d States of [Fe(bpy)$_3$]$^{2+}$. *J. Chem. Phys.* **2014**, *140*, 024309.

(51) Domingo, A.; Sousa, C.; de Graaf, C. The Effect of Thermal Motion on the Electron Localization in Metal-to-ligand Charge Transfer Excitations in [Fe(bpy)$_3$]$^{2+}$. *Dalton Trans.* **2014**, *43*, 17838–17846.

(52) Dorfman, K. E.; Bennett, K.; Mukamel, S. Detecting Electronic Coherence by Multidimensional Broadband Stimulated X-ray Raman Signals. *Phys. Rev. A: At., Mol., Opt. Phys.* **2015**, *92*, 023826.

(53) Zhang, Y.; Biggs, J. D.; Govind, N.; Mukamel, S. Monitoring Long-Range Electron Transfer Pathways in Proteins by Stimulated

Attosecond Broadband X-ray Raman Spectroscopy. *J. Phys. Chem. Lett.* **2014**, *5*, 3656−3661.

(54) Zhang, Y.; Biggs, J. D.; Hua, W.; Dorfman, K. E.; Mukamel, S. Three-dimensional Attosecond Resonant Stimulated X-ray Raman Spectroscopy of Electronic Excitations in Core-ionized Glycine. *Phys. Chem. Chem. Phys.* **2014**, *16*, 24323−24331.

(55) Kukura, P.; McCamant, D. W.; Mathies, R. A. Femtosecond Stimulated Raman Spectroscopy. *Annu. Rev. Phys. Chem.* **2007**, *58*, 461−488.

(56) Biggs, J. D.; Zhang, Y.; Healion, D.; Mukamel, S. Two-dimensional Stimulated Resonance Raman Spectroscopy of Molecules with Broadband X-ray Pulses. *J. Chem. Phys.* **2012**, *136*, 174117.

(57) Mukamel, S.; Healion, D.; Zhang, Y.; Biggs, J. D. Multidimensional Attosecond Resonant X-Ray Spectroscopy of Molecules: Lessons from the Optical Regime. *Annu. Rev. Phys. Chem.* **2013**, *64*, 101−127.

(58) Mitzner, R.; Rehanek, J.; Kern, J.; Gul, S.; Hattne, J.; Taguchi, T.; Alonso-Mori, R.; Tran, R.; Weniger, C.; Schröder, H.; et al. L-Edge X-ray Absorption Spectroscopy of Dilute Systems Relevant to Metalloproteins Using an X-ray Free-Electron Laser. *J. Phys. Chem. Lett.* **2013**, *4*, 3641−3647.

(59) Kubin, M.; Kern, J.; Gul, S.; Kroll, T.; Chatterjee, R.; Löchel, H.; Fuller, F. D.; Sierra, R. G.; Quevedo, W.; Weniger, C.; et al. Soft X-ray Absorption Spectroscopy of Metalloproteins and High-valent Metal-complexes at Room Temperature Using Free-electron Lasers. *Struct. Dyn.* **2017**, *4*, 054307.

(60) Gallo, E.; Glatzel, P. Valence to Core X-ray Emission Spectroscopy. *Adv. Mater.* **2014**, *26*, 7730−7746.

(61) Bauer, M. HERFD-XAS and Valence-to-core-XES: New Tools to Push the Limits in Research with Hard X-rays? *Phys. Chem. Chem. Phys.* **2014**, *16*, 13827−13837.

(62) Weninger, C.; Purvis, M.; Ryan, D.; London, R. A.; Bozek, J. D.; Bostedt, C.; Graf, A.; Brown, G.; Rocca, J. J.; Rohringer, N. Stimulated Electronic X-Ray Raman Scattering. *Phys. Rev. Lett.* **2013**, *111*, 233902.

(63) Kimberg, V.; Rohringer, N. Amplified X-Ray Emission from Core-Ionized Diatomic Molecules. *Phys. Rev. Lett.* **2013**, *110*, 043901.

(64) Weninger, C.; Purvis, M.; Ryan, D.; London, R. A.; Bozek, J. D.; Bostedt, C.; Graf, A.; Brown, G.; Rocca, J. J.; Rohringer, N. Stimulated Electronic X-Ray Raman Scattering. *Phys. Rev. Lett.* **2013**, *111*, 233902.

(65) Weninger, C.; Rohringer, N. Stimulated Resonant X-ray Raman Scattering with Incoherent Radiation. *Phys. Rev. A: At., Mol., Opt. Phys.* **2013**, *88*, 053421.

(66) Kimberg, V.; Rohringer, N. Stochastic Stimulated Electronic X-ray Raman Spectroscopy. *Struct. Dyn.* **2016**, *3*, 034101.

(67) Kimberg, V.; Sanchez-Gonzalez, A.; Mercadier, L.; Weninger, C.; Lutman, A.; Ratner, D.; Coffee, R.; Bucher, M.; Mucke, M.; Agåker, M.; et al. Stimulated X-ray Raman Scattering -A Critical Assessment of the Building Block of Nonlinear X-ray Spectroscopy. *Faraday Discuss.* **2016**, *194*, 305−324.